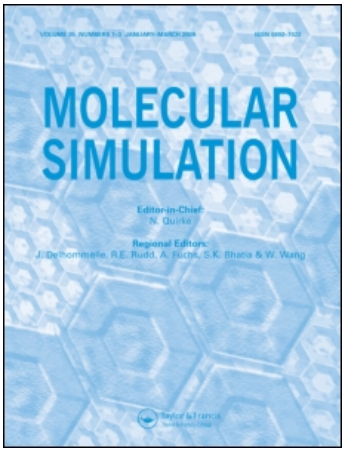

Molecular Simulation
Publication details, including instructions for authors and subscription information:
http://www.informaworld.com/smpp/title~content=t713644482

The Characterisation of Solids by Nuclear Magnetic Resonance and X-Ray Absorption Spectroscopy

Alan V. Chadwick[a]
[a] Centre for Materials Research, School of Physical Sciences, University of Kent, Kent, United Kingdom

To cite this Article Chadwick, Alan V.(1998) 'The Characterisation of Solids by Nuclear Magnetic Resonance and X-Ray Absorption Spectroscopy', Molecular Simulation, 21: 2, 105 — 126
To link to this Article: DOI: 10.1080/08927029808022054
URL: http://dx.doi.org/10.1080/08927029808022054

Molecular Simulation, 1998, Vol. 21, pp. 105–126
Reprints available directly from the publisher
Photocopying permitted by license only

THE CHARACTERISATION OF SOLIDS BY NUCLEAR MAGNETIC RESONANCE AND X-RAY ABSORPTION SPECTROSCOPY

ALAN V. CHADWICK

Centre for Materials Research, School of Physical Sciences, University of Kent, Canterbury, Kent CT2 7NR, United Kingdom

(Received October 1997; accepted January 1998)

The use of NMR and XAFS in characterising solids is described by the use of several examples. The examples are taken mainly from studies of ionic solids and include systems where the interpretation of the experimental data has strongly relied on guidance from the results of computer simulation studies. The examples include the study of diffusion in solids by NMR, structural studies of oxides by ^{17}O MAS-NMR and the location of dopant sites by EXAFS.

Keywords: NMR; EXAFS; ionic solids; diffusion; local structure

INTRODUCTION

The contributions at this meeting have covered the computer simulation of physical and chemical properties for a wide variety of solids. Two central issues have been the calculation of the structural details of materials and the modelling of the molecular motion. This contribution will focus on the role two experimental techniques, namely nuclear magnetic resonance (NMR) and X-ray absorption fine structure (XAFS), can play in providing information in these areas.

This paper is not meant to be a comprehensive review of the work that has been performed on the NMR and XAFS of solids. The objectives here are to (i) briefly outline the principles of the techniques, (ii) describe, by the use of appropriate examples, the information available from the experiments, and (iii) outline areas for future development. Due to the nature of the author's own research interests the examples will mainly be taken from studies of

defects and diffusion in ionic solids. An underlying theme of this contribution will be the links between these techniques and computer modelling. It will be demonstrated that these occur at various levels. The most ob- vious connection is the use of computer modelling to provide starting models for the interpretation of the experimental data. For example, the calculated energies of defect structures and processes will serve as a good guide to those which are feasible and those which can be neglected. In the later stages of data analysis it is often by an interplay of the computer modelling and the experiment that a final model of the process or structure is achieved. As both the experiments and the computer simulations become more sophisticated and the information revealed becomes more detailed in the future there will be even stronger contacts between the two approaches.

PRINCIPLES

Nuclear Magnetic Resonance

NMR spectroscopy is now an essential tool in modern chemistry and physics. The basic theory can be found in standard texts [1–4] and there are several books on pulsed experiments [5–7] and solid-state NMR [8]. The application of NMR in solid state diffusion has been reviewed by several authors [9–13]. It is only required here that a few fundamental concepts are recalled.

Consider a simple NMR experiment involving a liquid containing nuclei with spin I equal to 1/2 (*e.g.*, ^{1}H or ^{19}F) and magnetic moment μ, and all these nuclei are in the same chemical environment. The magnetogyric ratio γ is defined as μ/p, where p is the nuclear angular momentum $I\hbar$ and is a characteristic of the magnetic isotope. When the sample is placed in the field $\boldsymbol{B}_o$ of the spectrometer there are two quantum levels for the spins, the *Zeeman levels*, parallel and anti-parallel to $\boldsymbol{B}_o$, and the separation between these states is $\gamma\hbar\boldsymbol{B}_o$. In a continuous wave experiment the sample is subjected to an oscillating magnetic field $\boldsymbol{B}_1$ applied perpendicular to $\boldsymbol{B}_o$. As the frequency ω of the $\boldsymbol{B}_1$ field is swept absorption will occur at the resonance condition $\hbar\omega = \gamma\hbar\boldsymbol{B}_o$, and there will be excitation from the lower to upper spin states. This resonance frequency is the *Larmor precession frequency*, ω_o, equal to $\gamma\boldsymbol{B}_o$, and is in the radiofrequency range. In a liquid the absorption will be sharp, provided the $\boldsymbol{B}_o$ magnetic field is homogeneous, and the line will be narrow. This simple experiment is shown schematically in Figure 1.

In addition to the $\boldsymbol{B}_o$ field each nucleus will experience an additional local field, $\boldsymbol{B}_{\text{local}}$, arising from its local environment, *i.e.*, the local field from the

surrounding electrons and the neighbouring nuclear dipoles. In a liquid where all the nuclei are in the same chemical environment the rapid molecular motion will average out the $\boldsymbol{B}_{\text{local}}$ from the surrounding nuclei to zero and a sharp resonance line is observed. Again, in the case of a liquid sample, if there is more than one chemical environment for the nuclei (*i.e.*, in a polyatomic molecule) then there will be a series of sharp resonance lines at different frequencies, one for each environment. The shift of these lines from ω_o, the *chemical shift*, is a characteristic of the chemical environment and the magnitude of the line is proportional to the number of nuclei in that particular chemical environment. It is these two features that make NMR such an important analytical tool for chemists. In addition, at higher resolution the lines may be further split by interaction with nuclear spins on neighbouring positions of the same molecule.

In a rigid solid, even if all the nuclei are in the same chemical environment, the local dipolar field will vary from site to site causing a

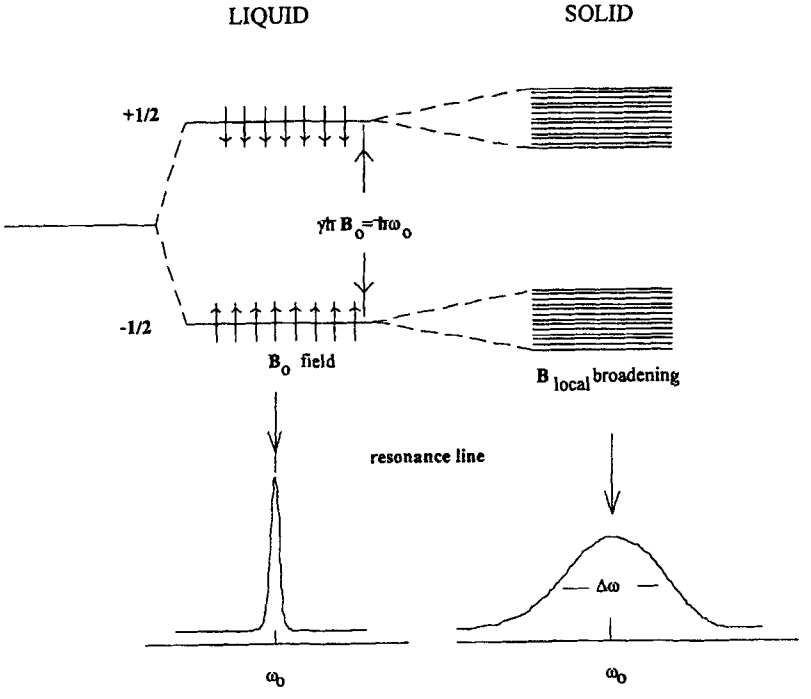

FIGURE 1 A schematic representation of the continuous wave experiment for a spin 1/2 nucleus. In liquids a sharp, narrow absorption line is observed at the Larmor frequency (on the left). In a solid the local dipolar fields from neighbouring nuclei split the quantum levels and the absorption line is broadened (on the right).

splitting of the quantum states and as a result the absorption line will be broadened, although still centred on ω_o. This broadening is large and will obscure the effects of the chemical shifts. This is also shown schematically in Figure 1.

The simple experiment outlined above is useful in recalling the basic ideas of NMR spectroscopy. Although the output from modern pulsed spectrometers will display the information in the form of a plot of absorption intensity *versus* frequency the method of operation is different. In this case the sample is subjected to an intense pulse of r.f. radiation rather than sweeping the $\boldsymbol{B}_o$ field. This causes excitation of the upper spin states and a change in the magnetisation of the sample. The change of magnetisation is then monitored as the system relaxes back to equilibrium. The Fourier transform (FT) of this signal from the time domain to the frequency domain will yield the 'normal' spectrum. The advantage of the use of FT-NMR is the achievement of a improved signal to noise ratio in a much shorter time than can be achieved by multiple sweeps of a $\boldsymbol{B}_1$ field.

Another important development in instrumentation is that of magic-angle-spinning (MAS) spectrometers. In these instruments the sample is mounted at an angle of 54.7° to the $\boldsymbol{B}_o$ field and spun rapidly. This has the effect of removing the dipolar field and as a result a high resolution spectrum can be observed for solid samples. The application of MAS-NMR in characterising solids is therefore similar to the use of high resolution liquid state NMR in chemistry. It is used to identify the chemical environments of species within the solid sample.

The effect of isotropic diffusional motion will be to average out the local fields causing the resonance line to narrow, an effect referred to as *motional narrowing*. The diffusion coefficient, D, is proportional to the reciprocal of the line-width, $1/\Delta\omega$, and line-width measurements can be used to estimate D. For diffusion involving a single mechanism D will follow a simple Arrhenius law, *i.e.*,

$$D = D_o \exp(-Q^*/kT) \tag{1}$$

where D_o is the pre-exponential factor and Q^* is the activation energy. Thus relatively accurate values of Q^* can be obtained from line-width measurements by plotting log $(\Delta\omega)$ *versus* $1/T$. This type of experiment is usually performed on an instrument capable of studying broad lines, although the lines can be sufficiently narrow in organic plastic solids for the measurements to be made on a high resolution spectrometer.

More precise studies of diffusion are possible by measuring the NMR relaxation times, T_1, T_2, $T_{1\rho}$ and T_{1D}. Briefly, the principle here is that the relaxation of spins between the quantum states depends on them being able to interact with oscillating magnetic fields at the appropriate resonance frequency. A source of oscillating fields is the diffusional motion of surrounding nuclear dipoles. The frequency distribution of these fields will depend on D. The difference between the different relaxation times is the magnitude of the separation between the quantum states in which the relaxation is occurring. Thus moving from T_1 and T_2 to $T_{1\rho}$ to T_{1D} there is an increasing sensitivity to slower motions. The range of diffusion coefficients that can be studied by NMR techniques is shown in Figure 2.

The exact relationship between the measured relaxation times and D requires the use of a theoretical model. The early BPP [14] model used to treat molecular motion in liquids has been adapted for solids [15, 16]. It is

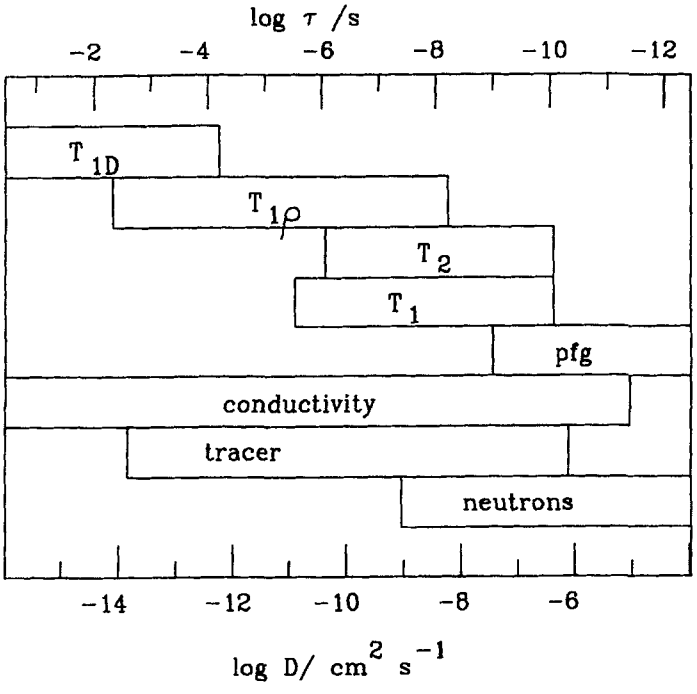

FIGURE 2 The typical range of diffusion coefficients that can be accessed by NMR techniques. The boxes are for the specific case of ^{19}F diffusion in the alkaline earth fluorides [22].

also necessary to account for correlation effects when the diffusion involves point defects. One effect is a *spatial* correction because not all the encounters of a nucleus and a defect result in displacement of the nucleus, an effect well known in radiotracer diffusion. A second effect is a *temporal* correction, arising because jumps within the encounter of a nucleus and a defect are too fast to cause relaxation and appreciable relaxation requires many encounters. These effects are included in the *encounter model* [17–20] and for cubic crystals exact values of D can be calculated from the measured relaxation times.

Finally, in this section it is worth mentioning the *pulsed field gradient* (pfg) NMR technique developed for diffusion in liquids [21] but useful for solids if diffusion is fast ($D > 10^{-13}\,m^2s^{-1}$) [22]. This is not a relaxation time measurement and it uses the nuclear spin as a label. The data analysis does not require the application of a theoretical model and the results are comparable to those from radiotracer measurements.

X-ray Absorption Spectroscopy

In X-ray absorption spectroscopy the absorption coefficient, μ (= log[*incident intensity/transmitted intensity*]) of a sample is measured as a function of the incident photon energy across the *absorption edge* for the ejection of a core level (K or L) electron. The typical spectrum for condensed matter is shown in Figure 3. Beyond the absorption edge there are oscillations referred to as *fine structure*. The whole region is referred to as *X-ray Absorption Fine Structure* (XAFS) and is divided into two regions, the *X-ray Absorption Near Edge Structure* (XANES) extending about 50 eV beyond the edge, and the *Extended X-ray Absorption Fine Structure* (EXAFS) extending typically 1000 eV beyond the edge. In addition, there can be pre-edge features in the spectrum. All these three types of feature provide structural information about the target atom, the atom which is emitting the photoelectron. The pre-edge features arise from excitations of the core electron to higher states within the atom and can fingerprint the oxidation state of the atom. In the XANES region the photoelectron is moving slowly and becoming involved with orbitals of the neighbouring atoms. This region provides a fingerprint for the oxidation state of the atom and its local coordination geometry. It is the oscillations in the EXAFS region that can be analysed in detail to provide quantitative information on the local environment. In this region the photoelectron is moving rapidly and is subject to single scattering events with the surrounding atoms. The theory of

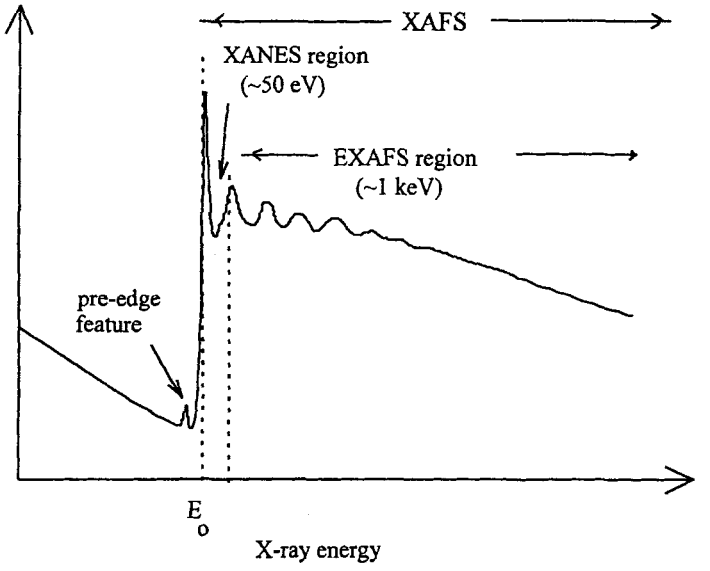

FIGURE 3 A typical X-ray absorption spectrum over the range for emission of a core (K or L) electron.

EXAFS can be found in several texts [23–26]. The oscillations arise from the photoelectron wave being backscattered and interfering with the outgoing wave. If the two waves are in phase there will be constructive interference, a lower final state energy and a higher probability for absorption. If the two waves are out of phase then there will be destructive interference, a higher final state energy and a lower probability for absorption. Thus as the incident photon energy increases so does the energy of the emitted photoelectron with consequential changes on its wavelength. Since the distance between the target atom and its neighbours is fixed there will be shifts in and out of phase and hence the observation of the EXAFS oscillations.

From the qualitative explanation in the preceding paragraph it should be clear that the frequency of the EXAFS oscillations contains information on the distance from the target atom from its neighbours. The intensity of the oscillations will depend on the type of atom which is acting as the backscatterer, *i.e.*, the higher the atomic weight the more intense the oscillations, and the number of backscattering atoms. To be more precise, after subtraction of the background absorption, the normalised absorption coefficient, $\chi(k)$, as a function of the photoelectron momentum, k, can be

written in an equation of the form [25, 27]:-

$$\chi(k) = \sum_j \frac{N_j}{kR_j^2} |f_j(\pi)| \exp(-2\sigma_j^2 k^2) \exp(-2R_j/\lambda) \sin(-2kR_j + \Psi_j + 2\delta) \tag{2}$$

Here N_j is the number of atoms (all of the same type) in shell j with backscattering factor $f_j(\pi)$ at a distance R_j from the central atom. The other terms in Eq. (2) are a Debye-Waller like factor σ_j expressing the mean square variation in R_j, the phase factors δ and Ψ_j of the photoelectron wave which depend on the central and scattering atom, and λ the mean free path of the photoelectron. The Fourier transform of $k \cdot \chi(k)$ with respect to $\sin(2kR)$ or $\exp(-2ikR)$ yields a partial radial distribution function in real space with peak areas proportional to N_j. If the phase factors are known, either from theoretical calculations or model compounds (*i.e.*, fitted from the EXAFS of chemically similar compounds to that under investigation but with known R_j and N_j), then the radial distances can be determined. The uncertainty in R_j that can be achieved with EXAFS is about ± 0.01Å. The determination of N_j is usually less accurate, about $\pm 20\%$, as it is strongly coupled to the Debye-Waller factor. $f_j(\pi)$ does not vary strongly with atomic number and the identification of the type of atoms in the shells is limited to differentiation between rows of the Periodic Table. The advantages of EXAFS over diffraction methods are that it does not depend on long range order, hence it can be used to study local environments in both crystalline and amorphous solids, and liquids, it is atom specific and can be sensitive to low concentrations of the target atom.

The set up of a typical XAFS experiment is shown schematically in Figure 4. The requirement of a high intensity, tuneable X-ray source means that the majority of experiments are now undertaken on synchrotron radiation sources. The experiment is basically simple. The white beam from the synchrotron is passed through a two crystal (usually silicon) monochromator, the wavelength being selected by the Bragg condition and step-wise rotation of the crystals allows a sweep of the X-ray energy. The intensity of the X-ray beam incident on the sample, I_o, is measured with an ion chamber filled with a gas mixture set to be 80% transmitting. For samples in which the target atom is concentrated (> 1%) a transmission mode is employed and the transmitted intensity, I_t, is measured with a second ion chamber, in this case set to be 80% absorbing. The absorption coefficient is simply evaluated from log (I_o/I_t). For dilute samples a fluorescence mode is used, where the fluorescence X-rays which are emitted upon absorption of the

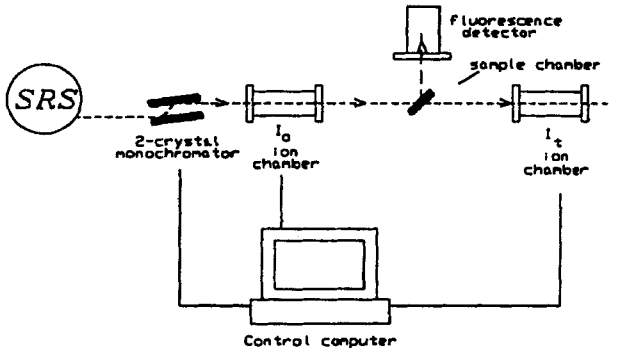

FIGURE 4 A sketch of the layout of a typical X-ray absorption station at a synchrotron source.

incident X-rays are used to monitor the absorption coefficient. A scan will typically take the order of 30 minutes. XAFS spectra can be collected for most elements in the Periodic Table, however for the lighter elements (roughly those lighter than calcium) air absorption will significant and the sample needs to be in a vacuum along with the X-ray beam.

EXAFS data analysis is performed with interactive computer programmes, such as the EXCALIB, EXBACK and EXCURVE codes developed at the Daresbury SRS [28] or the University of Washington codes, UWAXFS [29]. The final step in the procedure is least-squares fitting the data to a model of the local structure with parameters such as N_j, R_j and σ_j as variables. In simple cases the choice of the model can be made from intuition. In more complex systems computer simulations play a vital role in providing suitable starting models for the fitting.

EXAMPLES OF APPLICATIONS

Nuclear Magnetic Resonance

Diffusion Studies

NMR measurements have been extensively used to study diffusion in rare gas solids [30] and the class of molecular solids known as *plastic crystals* [31]. In these latter materials the molecules are globular-shaped and are undergoing rapid endospherical reorientation. The crystal structures are symmetric close-packed (cubic or hexagonal) and diffusion is relatively fast.

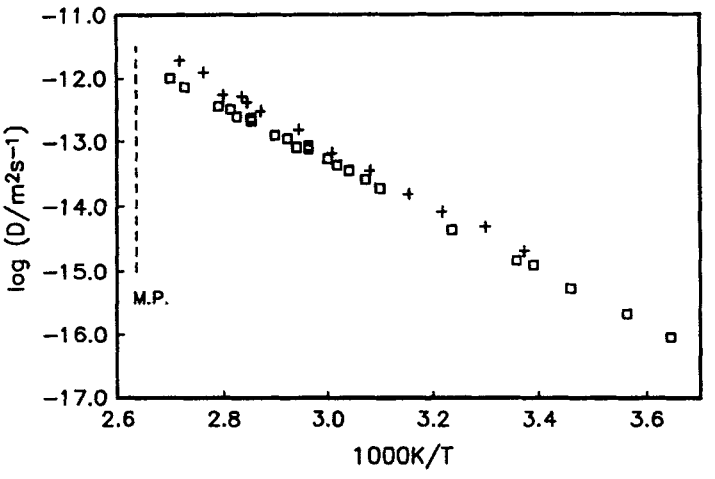

FIGURE 5 Self-diffusion coefficients in solid hexamethylethane (2,2,3,3-tetramethylbutane); □, NMR measurements [32]; +, radiotracer measurements [33]. The NMR values were evaluated using the Wolf encounter model.

An excellent example of the use of NMR is displayed in Figure 5, which shows the values of D for the plastic solid hexamethylethane, (2, 2, 3, 3-tetramethylbutane, $((CH_3)_3—C—C—(CH_3)_3)$, from relaxation time measurements [32] and from radiotracer studies [33] (which is generally regarded as the most reliable diffusion technique). The agreement is the two sets of data is within the experimental error. Similar agreement is found for a large number of plastic crystals, however it should be noted there are some notable exceptions [31].

An extremely thorough study was made of F^- diffusion in BaF_2 using NMR methods by Figueroa *et al.* [34]. ^{19}F relaxation time measurements were collected over a wide temperature range for a series of pure and doped single crystals. Diffusion coefficients were evaluated using the Wolf encounter model [18–20] and compared with values calculated from ionic conductivity measurements collected for the *same crystals*. It is important to note that the dopants that were used, K^+, La^{3+} and O^{2-} are not paramagnetic. Examples of the data are shown in Figure 6. The data were subjected to a very detailed analysis and compared the results from computer simulations assuming various defect models. It was possible to prove that the intrinsic defects were anion-Frenkel pairs and that the more mobile defect was the F^- vacancy. In addition, precise values of the defect energies were derived.

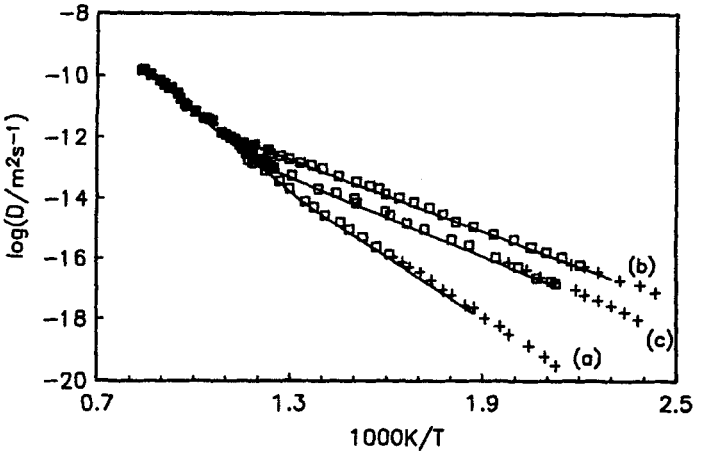

FIGURE 6 Fluorine self-diffusion coefficients in BaF_2 single crystals [34]; (a) pure, (b) doped with 0.04 mole percent KF, (c) doped with 0.05 mole percent LaF_3. The lines are from ionic conductivity measurements on the crystals and the NMR points are from T_{1D}(+), $T_{1\rho}$ (□) and T_1(■) measurements.

The excellent agreement between NMR and conductivity for BaF_2, *i.e.*, concurrence of the data over nine orders of magnitude, emphasises the power of relaxation time measurements for diffusion studies. However, the system was almost ideal in that ^{19}F has a strong NMR signal and is 100% abundant, single crystals were employed and the level of paramagnetic impurities was extremely low. Paramagnetic impurities are a lesser problem for pfg-NMR diffusion measurements and these were used to study F^- diffusion in the high temperature, fast-ion region of PbF_2. There were reports that the diffusion as measured by relaxation time measurements was considerable slower than that measured by conductivity methods [35]. However, at high temperatures very small amounts of paramagnetic impurities will affect the NMR relaxation times [36]. When pfg-NMR data were collected for this system [37, 38] it was found there was a good agreement with the conductivity results, as is shown in Figure 7. This was important in that it indicates a vacancy mechanism is operative in the fast-ion phase.

Structural Studies

As pointed out above key features of MAS-NMR are the position of the resonance line is an indication of the chemical environment and the intensity of the line is a measure of the fraction of nuclei in that particular

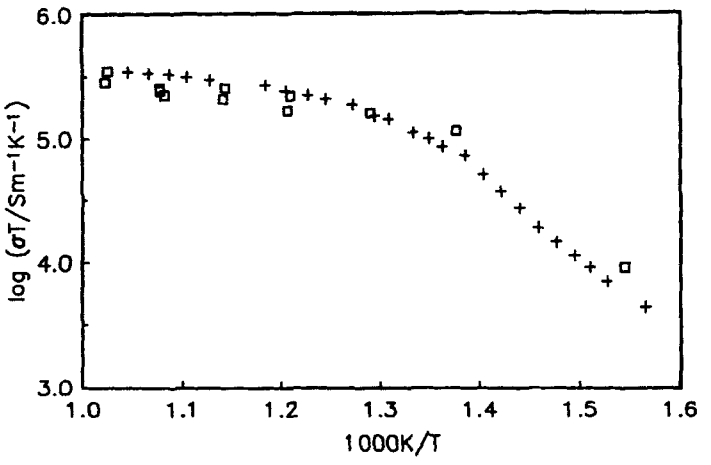

FIGURE 7 The temperature dependence of the ionic conductivity of β-PbF_2 in the fast ion region [37, 38]; +, conductivity measurements, □, the conductivity calculated from the pfg-NMR diffusion coefficients assuming an F^- vacancy mechanism of conduction.

environment. This has proved particularly useful in structural studies of silicates and aluminosilicates [8, 39], where the materials are important catalysts. Many of these materials are microcrystalline, precluding the use of conventional diffraction method, and ^{29}Si and ^{27}Al NMR have provided a vital structural tool.

The example chosen here is the use of ^{17}O MAS-NMR in the study of the sol-gel preparation of special glasses [40]. ^{17}O has a large chemical shift range and although $I = 5/2$ the quadrupolar interaction is modest. Therefore it can be more informative than ^{29}Si NMR as shifts are based on *nn* interactions rather than *nnn* interactions. In particular, it has been found that Ti—O—Ti and Si—O—Si linkages have very different ^{17}O chemical shifts (500–600 ppm and 30–90 ppm, respectively) [41]. In addition, OTi_3 and OTi_4 can be readily distinguished (shifts of $\sim$530 and $\sim$370 ppm, respectively) [41, 42]. However, ^{17}O has a low sensitivity and a very small natural abundance (0.037%), requiring samples to be isotopically enriched.

Titania-silica mixed oxides are technologically important as they are used in the optical industry to form films with tailored refractive indices [43], they form ultra-low expansion glasses [44] and they are used as catalyst supports [45]. Homogeneity at the atomic level is important in the applications of these materials. Sol-gel synthesis is a good route to these systems, however careful control of conditions is required to form homogeneous material. The

presence of peaks in the ^{17}O around 530 and 370 ppm can be used to fingerprint OTi_3 and OTi_4 and provide evidence of phase separation [40]. In addition, the peak around 280 ppm was identified as due to Si—O—Ti linkages and a small intensity of this signal is a further test of phase separation [40]. Using these tests the conditions were determined for the preparation of samples intimately mixed at the atomic level.

X-ray Absorption Spectroscopy

There are several good examples of the use of EXAFS to locate the sites occupied by dopants in solids, particularly ionic materials [46, 47]. The rather complex situation of rare-earth doped CaF_2 was resolved by a combination of neutron diffraction, computer modelling and EXAFS [48–50]. The position of the additional vacancies created by rare-earth doping ZrO_2 was the cause of considerable debate and they were shown be EXAFS [51] to be predominantly adjacent to the Zr^{4+} ions rather than the dopant. Again the analysis was aided by computer simulation work [52] and has been supported by more recent, very detailed EXAFS experiments [53]. Similarly, the transition metal dopants in $LiNbO_3$ were shown by EXAFS to predominantly to substitute on the Li site rather than the Nb site, ending a long run- ning controversy [54–56]. Two more recent examples will be used here to demonstrate the application of EXAFS.

$BaLiF_3$ is a new material that has potential technological applications when doped with divalent cations. The most important use would be as a tuneable vibronic laser material in the near infrared region (around 1.5μm) suitable for telecommunication devices. The crystal structure of $BaLiF_3$ [57] can be viewed as an inverted fluoroperovskite where the cations Ba^{2+} and Li^+ occupy inverted positions as compared with other fluoroperovskites like $KMgF_3$. It belongs to the space group *Pm3-m* where both the Ba^{2+} and the Li^+ sites have cubic symmetry (O_h) but the coordination number is 6 for the Li^+ site and 12 for the Ba^{2+} site. The lattice parameter is 3.995 Å [4] and the unit cell is shown in Figure 8.

The positions of dopant divalent cations were a matter of debate although some indirect evidence from optical studies suggests that Ni^{2+} ions are in a local octahedral environment, *i.e.*, on the Li^+ site of the host lattice. Static-lattice energy minimisation atomistic simulations predicted that the lowest energy site for Ni^{2+} substitution was the Li^+ site [58]. The crystallographic data suggested that if the Ni^{2+} ion predominantly occupies either a Li^+ or a Ba^{2+} site in $BaLiF_3$ the two possibilities should be readily resolved by the

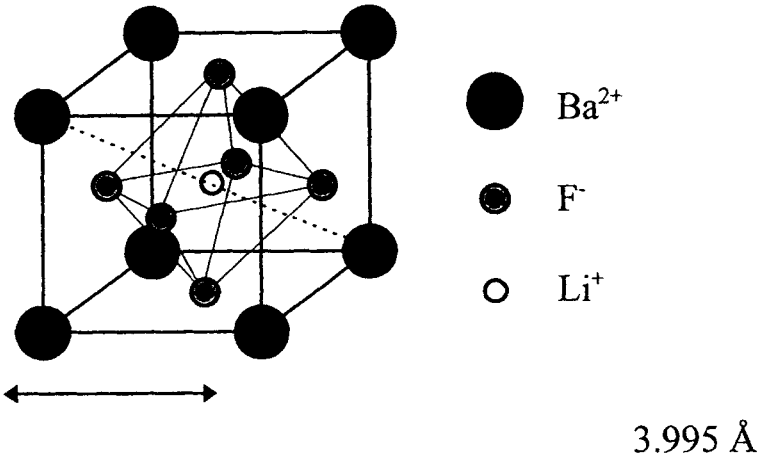

FIGURE 8 The unit cell of $BaLiF_3$.

EXAFS technique. The local site geometries are very different, in particular there are large differences in the numbers and distances of the nearest F^- neighbours. The Li^+ site is surrounded by six F^- ions at 1.998 Å whereas the Ba^{2+} site is surrounded by 12 F^- ions at 2.825Å.

The fluorescence Ni K-edge EXAFS were collected for a crystal of $BaLiF_3$doped with 0.95 mole per cent Ni^{2+} at the Daresbury SRS [59]. The EXAFS and the Fourier transforms are displayed in Figures 9 and 10. In Figure 9 the data are compared with a model in which the Ni occupies the Li site, whereas the model employed in Figure 10 is Ni occupying the Ba site. A simple visual comparison immediately indicates that the closest fit is for the first of these models. The frequency and magnitude of the oscillations of the raw data are well matched by the model in Figure 9. The analysis was taken beyond this fingerprinting approach and the parameters were refined to yield the least-squares best-fit values shown in Table I. It was possible to estimate that at least 85% of the Ni was on the Li sites [59]. Thus there was excellent accord with the computer simulations [58]. The preference for the Li site is a result of the better match of the ionic radii (Ni^{2+} 0.69 Å, Li^+ 0.90 Å, Ba^{2+} 1.49 Å) and the provision of octahedral symmetry which is common in other Ni–F structures. Finally it is worth noting that the Debye-Waller factors for the shells beyond the nearest neighbour F shells are rather large. This is presumably due to the presence of charge-compensating defects in the region of the Ni which would not easily be distinguished in the EXAFS, but which have been studied by computer modelling [58].

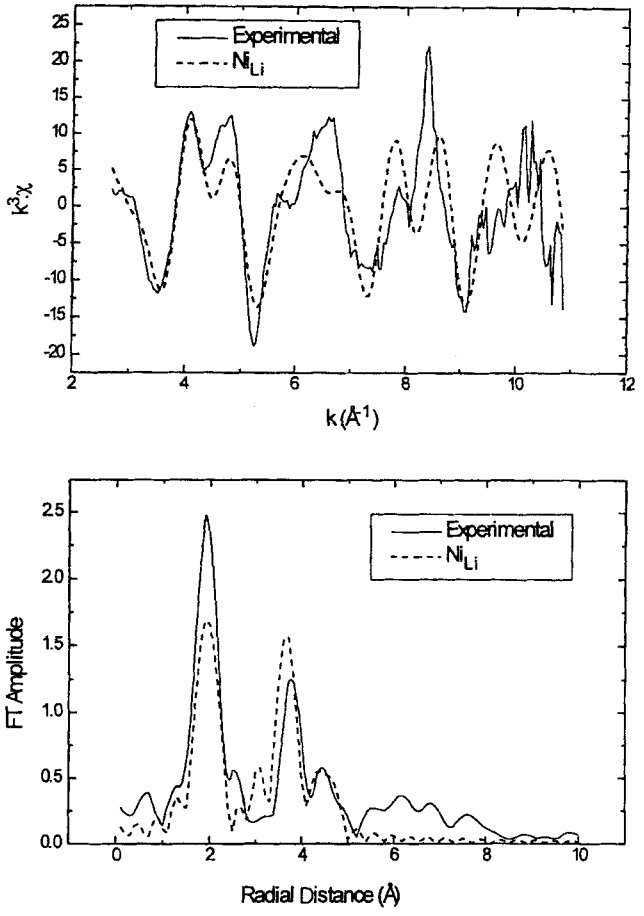

FIGURE 9 The Ni K-edge EXAFS for Ni doped $BaLiF_3$ assuming a model of simple substitution on Li site. The upper plot is the normalised EXAFS (k^3 weighted) and the lower plot is the Fourier transform (phase shifted with respect to the first shell). The solid line is the experimental and the dashed line the model. The Debye-Waller factors were set at a default value, $2\sigma^2 = 0.01$.

The second example comes from a recent study of doped nanocrystalline tin oxide [60]. Tin oxide is extensively used as the working element in gas sensors and considerable effort is going into the improvement of their sensitivity and selectivity [61, 62]. Several strategies are employed including the use of nanocrystalline materials and the addition of cationic dopants. Nanocrystalline doped with copper and iron was studied on station 9.3 at the Daresbury SRS. This station allows the simultaneous collection of both EXAFS and X-ray powder diffraction patterns, and is equipped with an

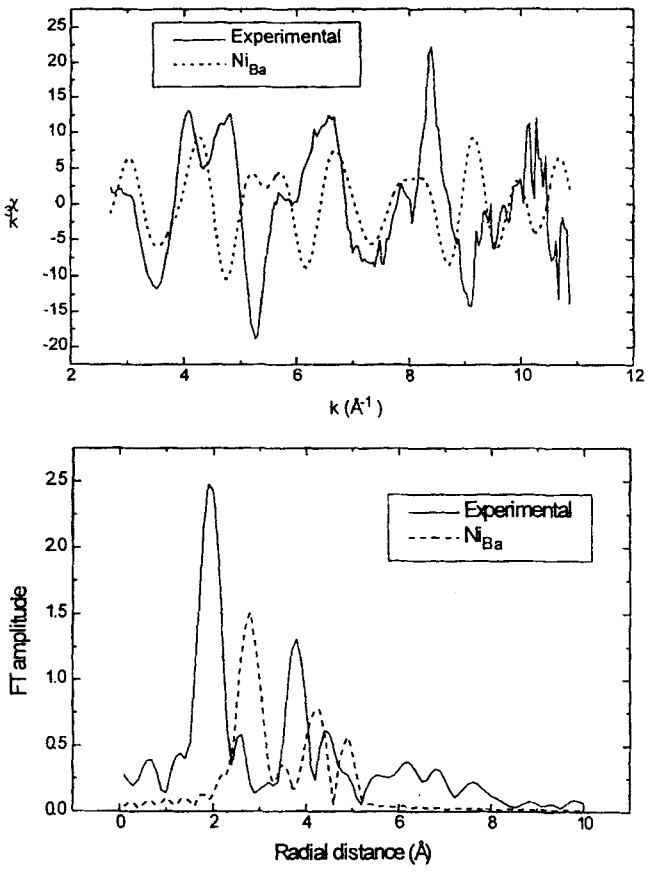

FIGURE 10 The Ni K-edge EXAFS for Ni doped $BaLiF_3$ assuming a model of simple substitution on Ba- site. The upper plot is the normalised EXAFS (k^3 weighted) and the lower plot is the Fourier transform (phase shifted with respect to the first shell). The solid line is the experimental and the dashed line the model. The Debye-Waller factors were set at a default value, $2\sigma^2 = 0.01$.

environmental chamber that allows the sample to be studied from room temperature to 1100°C [63]. The data for the copper doped samples will be discussed here.

Nanocrystalline tin oxide nominally doped with 5 mole per cent Cu was prepared by a sol-gel technique [60]. From the broadening of the X-ray powder pattern peaks the average particle size was 2 to 3 nm. Cu K-edge EXAFS and diffraction data were collected on samples that been annealed for one hour at a series of temperatures. The EXAFS of the as-prepared sample is shown in Figure 11. There are two dominant peaks, one at ~ 2 Å

TABLE I The best-fit structural model to the Ni K-edge EXAFS: The model assumes the Ni^{2+} substitutes on the Li^{+} site. Coordination numbers were not iterated in the fitting. The distances listed in square brackets are the distances from a Li^{+} ion in pure $BaLiF_3$ from crystallographic data

Atom	*Coordination*		
	CN	$R/\AA$	$2\sigma^2/\AA^2$
F^-	6	1.977 ± 0.002 [1.998]	0.0033 ± 0.0004
Ba^{2+}	8	3.554 ± 0.005 [3.460]	0.0182 ± 0.0009
Li^+	6	4.083 ± 0.109 [3.995]	0.0200 ± 0.0111
F^-	24	4.486 ± 0.007 [4.665]	0.0181 ± 0.0020

CN = coordination number, r = radial distance, σ = Debye-Waller factor.

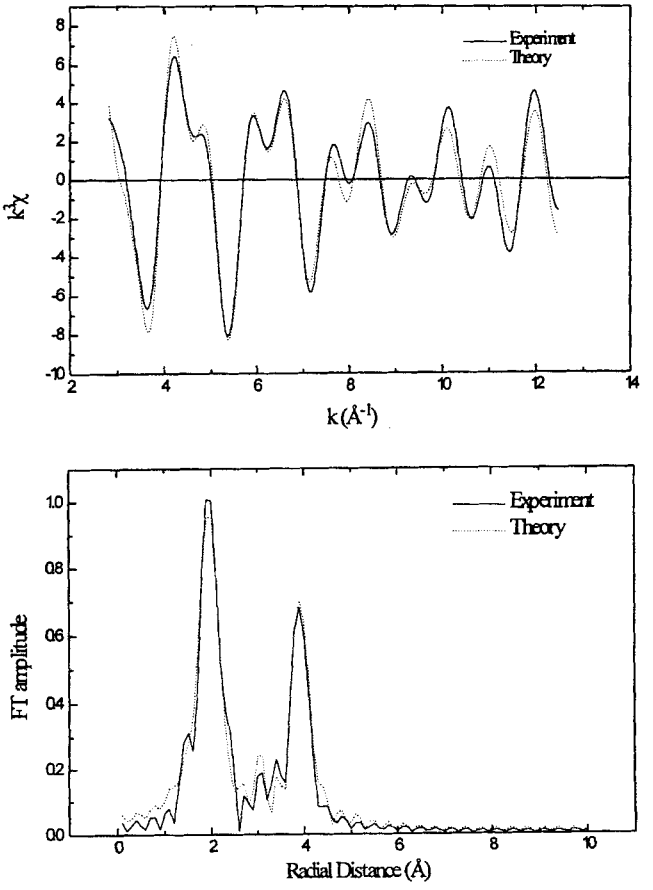

FIGURE 11 The Cu K-edge EXAFS for for as-prepared, nominally 5 mole per cent Cu doped nanocrystalline SnO_2. The upper plot is the normalised EXAFS (k^3weighted) and the lower plot is the Fourier transform (phase shifted with respect to the first shell). The solid line is the experimental and the dashed line the model using the parameters in Table II.

TABLE II EXAFS results for as-prepared, nominally 5 mole per cent Cu doped nanocrystalline tin oxide

Atom	*X-ray for SnO_2*		*Cu K-edge EXAFS of 5% Cu-SnO_2 **		
	CN	*R/Å*	*CN*	*R/Å*	$2\sigma^2/Å^2$
O	2	2.045	6	1.995	0.017
O	4	2.088			
Sn	2	3.185	2	3.150	0.013
O	4	3.594	4	3.618	0.011
Sn	8	3.708	8	3.637	0.018

*The crystallographic data for CuO shows the shell around Cu^{2+} are (number of atoms,atom type, distance/Å):- 2[O] 1.951;2[O] 1.961;2[O] 2.781;4[Cu] 2.900;4[O] 3.083;2[Cu] 3.172;2[0] 3.408;2[Cu] 3.421;2[O] 3.580; 2[Cu] 3.749;2[O] 3.873.

and one at ~ 4 Å, due to backscattering from oxygen and metal atoms, respectively. It is clear that the Cu has dissolved into the SnO_2 lattice as the spectrum is very different to that for CuO. In CuO a large peak at around 3 Å is seen in the Fourier transform of the Cu K-edge EXAFS due to a shell of ten cations between 2.9 and 3.2 Å. The data in Figure 11 fits very well to a model that assumes the Cu has substituted randomly on the Sn sites. The results of the detailed analysis of these data are shown in Table II. The effect on the EXAFS of annealing the sample at various temperatures is displayed in Figure 12. It can be seen that the peak at 4 Å, due to the shell of Sn atoms, decreases with increasing annealing temperature. The diffraction data show

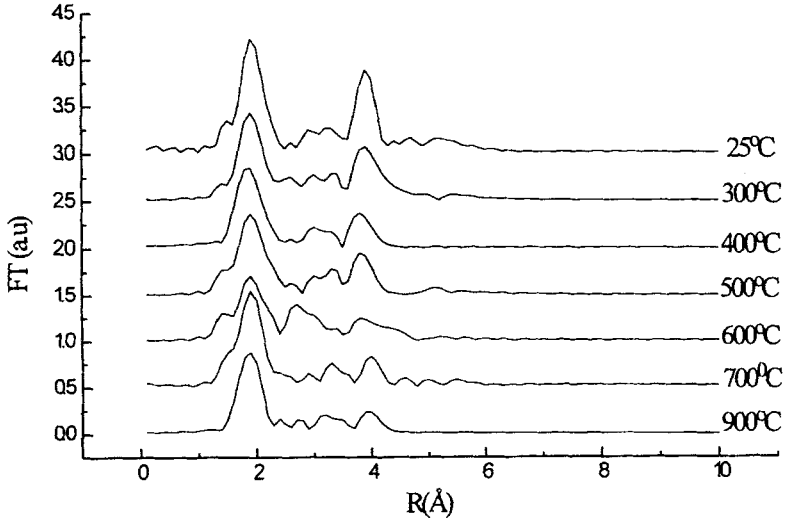

FIGURE 12 The Fourier transform of the Cu K-edge EXAFS of 5 mole percent Cu doped nanocrystalline tin oxide annealed for one hour at the temperatures indicated. The plots have been displaced by 5 units for clarity.

that at 400°C the particles begin to increase in size and this growth accelerates rapidly as the temperature increases, to the extent that a one hour anneal at 900°C yields an average particle size of ~ 50 nm.

The annealing of the sample is clearly changing the local environment of the Cu and it is becoming located in a more disordered site. It was suggested [60] that this site is within the surface regions of the SnO_2 crystallites. This has implications for the use of nanocrystalline SnO_2 in gas sensors. The sensitivity has an inverse relationship to particle size and is highest for crystallites less than 10 nm diameter, the order of the Debye length in SnO_2 [64]. A compromise therefore has to be reached, if possible, where the temperature of sensor operation is sufficient to give a sensitivity to gas without crystallite growth and a re-distribution of the dopant.

SUMMARY

The series of experiments described above demonstrate the application of NMR and EXAFS in characterising the diffusion and local structure of solids. In each case the techniques that were used are now well-established. It is worth considering at this stage the recent developments that have occurred in this area of research and what new experiments might be possible in the near future.

There are continuing developments in NMR spectrometers and instrumentation that are widening the number of elements that can be studied. The use of ^{17}O in MAS-NMR has proved to be an invaluable tool in the study of oxides and similar developments are to be expected for other nuclei. Similarly NMR diffusion studies have mainly been restricted to the more accessible nuclei (like ^{1}H and ^{19}F) but could now be extended to others. The potential of using ^{17}O in self-diffusion studies of oxides has been successfully demonstrated in ceria [65] and should find wider usage for monitor oxygen diffusion as there is no suitable radiotracer for this element. The pfg-NMR technique is finding wider usage but the requirement of relatively fast diffusion is a limitation. Recently a variation of the method, referred to as the *fringe field* approach to field gradient diffusometry, has been developed mainly for the study of polymers (notably by Kimmich and co-workers [66]). This extends the lower D value that can be measured by about one order of magnitude [67] and could prove very useful for solids.

In the last few years there have been several developments in the instrumentation for X-ray absorption spectroscopy. Many of these developments, such as increased intensities at synchrotron sources, improved

detectors and rapid scanning monochromators, have reduced the data collection time for the spectrum and have led to 'quick' EXAFS or QUEXEFS, with spectra measured in the matter of seconds or less. Thus it is now possible to study with EXAFS the kinetics of structural changes that occur during phase transitions or chemical reactions. Improved intensity and detection also means lower concentrations of atoms can be studied and 'high dilution EXAFS' stations, such as station 16.5 at the Daresbury SRS, are being commissioned. This is particularly important in the study of dopant environments in solids and comparing the experiments with the results of computer modelling. The latter approach usually simulates the case of a single impurity atom in a host lattice, *i.e.*, infinite dilution, and hence the lower the concentration in the experiment then the more realistic will be the comparison.

Finally it is worth noting that the most exciting development for materials scientists at synchrotron sources is the construction of 'combined' stations'. An example is station 9.3 at the Daresbury SRS which allows simultaneous collection of EXAFS and powder X-ray diffraction patterns, providing information on both short range and long range order. The data for SnO_2 described above were collected on this station. As the time of EXAFS data collection is reduced a variety of other techniques can be combined with EXAFS to provide extra information on the system and possibilities include calorimetric measurements, optical studies and kinetic investigations.

Acknowledgements

The author would like to express his thanks to Professor John Strange for his advice on NMR techniques and continuing support during many years of collaboration. Thanks are also due to many postgraduate students at Kent who have been involved in this work, particularly Steven Davis who was involved in the EXAFS work on $BaLiF_3$ and SnO_2. The research has been supported by the EPSRC and the help of staff of the Daresbury SRS is gratefully acknowledged.

References

[1] Abragam, A. (1961). "The Principles of Nuclear Magnetism", Oxford University Press, London.
[2] Slichter, C. P. (1975). "The Principles of Magnetic Resonance", Harper and Row, New York.
[3] Goldman, M. (1970). "Spin Temperature and Nuclear Magnetic Resonance in Solids", Oxford University Press, London.

[4] Hennel, J. W. and Klinowski, J. (1993). "Fundamentals of Nuclear Magnetic Resonance", Longman Scientific and Technical, Harlow.
[5] Farrar, T. C. and Becker, E. D. (1971). "Pulse and Fourier Transform NMR", Academic Press, New York.
[6] Fukushima, E. and Roeder, S. B. W. (1981). "Experimental Pulse NMR A Nuts and Bolts Approach", Addison-Wesley, Reading, Mass.
[7] Harris, R. K. (1983). "Nuclear Magnetic Resonance Spectroscopy", Pitman, London.
[8] Fyfe, C. A. (1983). "Solid State NMR for Chemists", CFC Press, Guelph.
[9] Strange, J. H. (1986). In "Defects in Solids – Modern Techniques", Chadwick, A. V. and Terenzi, M., Eds., Plenum Press, New York, p. 243.
[10] Kanert, O. (1982). *Phys. Rep.*, **91**, 183.
[11] Ailion, D. C. (1983). In: "Methods in Solid State Physics; 21, Nuclear Methods", Mundy, J. N., Rothman, S. J., Fluss, M. J. and Smedskjaer, L. C., Eds., Academic Press, New York, p. 439.
[12] Chadwick, A. V. (1988). *Int. Rev. Phys. Chem.*, **7**, 251.
[13] Chadwick, A. V. (1990). *J.C.S. Faraday Trans.*, **86**, 1157.
[14] Bloembergen, N., Purcell, E. M. and Pound, R. V. (1948). *Phys. Rev.*, **73**, 679.
[15] Torrey, H. C. (1953). *Phys. Rev.*, **92**, 962.
[16] Torrey, H. C. (1954). *Phys. Rev.*, **96**, 690.
[17] Eisenstadt, M. and Redfield, A. G. (1963). *Phys. Rev.*, **132**, 635.
[18] Wolf, D. (1974). *Phys. Rev. B*, **10**, 2710.
[19] Wolf, D. (1974). *Phys. Rev. B*, **10**, 2724.
[20] Wolf, D. (1979). "Spin Temperature and Nuclear Magnetic Resonance", Clarendon Press, Oxford.
[21] Stejskal, E. O. and Tanner, J. E. (1965). *J. Chem. Phys.*, **42**, 288 .
[22] Gordon, R. E. and Strange, J. H. (1979). *Faraday Symp. Chem. Soc.*, **13**, 154 .
[23] Teo, B. K. and Joy, D. C. Eds. (1980). "EXAFS Spectroscopy; Techniques and Applications", Plenum Press, New York.
[24] Hayes, T. M. and Boyce, J. B. (1982). *Solid State Phys.*, **37**, 173.
[25] Koningsberger, D. C. and Prins, R., Eds. (1988). "X-ray Absorption", Wiley, New York.
[26] Catlow, C. R. A. and Greaves, G. N., Eds. (1990) "Applications of Synchrotron Radiation", Blackie, Glasgow.
[27] Lee, P. A. and Pendry, J. B. (1975). *Phys. Rev. B*, **11**, 2795.
[28] Binsted, N., Campbell, J. W., Gurman, S. J. and Stephenson, P. C. (1992). EXCURV92 Programme, SERC Daresbury Laboratory, Warrington WA4 4AD, Cheshire, U.K.
[29] Stern, E. A., Newville, M., Ravel, B., Yacoby, Y. and Haskel, D. (1995). *Physica B*, **209**, 117.
[30] Chadwick, A. V. (1983). In: "Matter transport in solids", Beniere, F. and Catlow, C. R. A., Eds., Plenum Press, New York, p. 285.
[31] Boden, N. (1979). In: "The Plastically Crystalline State", Sherwood, J. N., Ed., Wiley, New York, p. 147.
[32] Britcher, A. R. and Strange, J. H. (1979). *Mol. Phys.*, **37**, 181 (1979).
[33] Lockhart, N. C. and Sherwood, J. N. (1972). *Faraday Symp. Chem. Soc.*, **6**, 57
[34] Figueroa, D. R., Chadwick, A. V. and Strange, J. H. (1978). *J. Phys. C*, **11**, 55.
[35] Boyce, J. B., Mikkelsen, J. C. and O'Keeffe, M. (1977). *Solid State Comm.*, **21**, 955.
[36] Hogg, R. D., Vernon, S. P. and Jaccarino, V. (1977). *Phys. Rev. Lett.*, **39**, 481.
[37] Gordon, R. E. and Strange, J. H. (1978). *J. Phys. C*, **11**, 3213.
[38] Carr, V. M., Chadwick, A. V. and Saghafian, R. (1978). *J. Phys. C*, **11**, L637.
[39] Yannoni, C. S. (1982). *Acc. Chem. Res.*, **15**, 201.
[40] Dirken, P. J., Smith, M. E. and Whitfield, H. J. (1995). *J. Phys. Chem.*, **99**, 395.
[41] Day, V. W., Eberspracher, W. G., Klemperer, C. W., Park, C. W. and Rosenberg, F. S. (1992). In: "Chemical Processing of Advanced Materials", Hench, L. L. and West, J. K., Eds., Wiley, New York.
[42] Smith, M. E. and Whitfield, H. J. (1994). *J. Chem. Soc. Chem. Comm.*, 723.
[43] Schultz, P. C. and Smyth, H. Y. (1972). In: "Amorphous Materials", Douglas, E. W. and Ellis, B., Eds., Wiley, London.
[44] Brinker, C. J. and Scherer, G. W. (1990). "Sol-Gel Science; the Physics and Chemistry of Sol-gel Processing", Academic, San Diego.

[45] Itoh, M., Hattori, H. and Tanabe, K. (1974). *J. Catalysis*, **35**, 225.
[46] Chadwick, A. V. (1993). *Solid State Ionics*, **63–65**, 721.
[47] Chadwick, A. V. (1990). In: "Application of Synchrotron Radiation", Catlow, C. R. A. and Greaves, G. N., Eds., Blackie, Glasgow, p. 171.
[48] Catlow, C. R. A., Chadwick, A. V., Greaves, G. N. and Moroney, L. M. (1984). *Nature*, **312**, 601.
[49] Catlow, C. R. A., Chadwick, A. V., Greaves, A. V. and Moroney, L. M. (1985). *Crystal Latt. Def. and Amorph. Mat.*, **12**, 193.
[50] Catlow, C. R. A., Chadwick, A. V., Corish, J., Moroney, L. M. and O'Reilly, A. N. (1989). *Phys. Rev. B*, **29**, 1897.
[51] Catlow, C. R. A., Chadwick, A. V., Moroney, L. M. and Greaves, G. N. (1986). *J. Amer. Ceram. Soc.*, **69**, 272.
[52] Catlow, C. R. A., Chadwick, A. V., Cormack, A. N., Greaves, G. N., Leslie, M. and Moroney, L. M. (1986). Defect properties and processing of high-technology non-metallic materials, pp. 173–178.
[53] Li, P., Chen, I. W. and Penner-Hahn, J. E. (1993). *Phys. Rev. B*, **48**, 10082.
[54] Prieto, C., Zaldo, C., Fessler, P., Dexpert, H., Sanz-Garcia, J. A. and Diequez, E. (1991). *Phys. Rev. B*, **43**, 2594.
[55] Catlow, C. R. A., Chadwick, A. V., Cole, M. and Tomlinson, S. M. (1991). *Radiat. Eff. Def. Solids*, **119**, 565.
[56] Bush, T. S., Catlow, C. R. A., Chadwick, A. V., Cole, M., Geatches, R. M., Greaves, G. N. and Tomlinson, S. M. (1992). *J. Mater. Chem.*, **2**, 309.
[57] Baldochi, S. L. and Gessland, J. Y. (1992). *Mat. Res. Bull.*, **27**, 891.
[58] Jackson, R. A., Valerio, M. E. G. and de Lima, J. F. (1997). *J. Phys.– Condensed Matter*, **8**, 10931.
[59] Chadwick, A. V., Davis, S. R., de Lima, J. F., Valerio, M. E. G. and Baldochi, S. (1996). *J. Phys.– Condensed Matter*, **8**, 10679.
[60] Davis, S. R., Chadwick, A. V. and Wright, J. D. (1997). *J. Phys. Chem. B*, **101**, 9901.
[61] Lantto, V. (1992). In: "Gas Sensors; Principles, Operations and Developments", Sberveglieri, G., Ed., Kluwer, Dordrecht, p. 117.
[62] Williams, D. E. (1987). In: "Solid State Gas Sensors", Moseley, P. T. and Tofield, B. C., Eds., Adam Hilger, Bristol, p. 71.
[63] Dent, A. J., Oversluizen, M., Greaves, G. N., Roberts, M. A., Sankar, G., Catlow, C. R. A. and Thomas, J. M. (1995). *Physica*, **209**, 253.
[64] Xu, C., Tamaki, J., Miura, N. and Yamazoe, N. (1990). *Chem. Lett.*, p. 441.
[65] Fuda, K., Kishio, K., Yamauchi, S., Fueki, K. and Onoda, Y. (1984). *J. Phys. Chem. Solids*, **45**, 1253.
[66] Fischer, E., Kimmich, R. and Fatkullin, N. (1996). see, for example, *J. Chem. Phys.*, **104**, 9174.
[67] Strange, J. H., Private Communication.